INTERNATIONAL JOURNAL FOR NUMERICAL METHODS IN FLUIDS
Int. J. Numer. Meth. Fluids 2001; **37**: 885–903 (DOI: 10.1002/fld.195)

Higher-order finite element discretizations in a benchmark problem for incompressible flows

Volker John*,[1] and Gunar Matthies

Otto-von-Guericke-Universität Magdeburg, Institut für Analysis und Numerik, Magdeburg, Germany

SUMMARY

We present a numerical study of several finite element discretizations applied to a benchmark problem for the two-dimensional steady state incompressible Navier–Stokes equations defined in Schäfer and Turek (The benchmark problem 'Flow around a cylinder'. In *Flow Simulation with High-Performance Computers II. Notes on Numerical Fluid Mechanics*, vol. 52, Hirschel EH (ed.). Vieweg: Wiesbaden, 1996; 547–566). The discretizations are compared with respect to the accuracy of the computed benchmark parameters. Higher-order isoparametric finite element discretizations turned out to be by far the most accurate. The discrete systems obtained with higher-order discretizations are solved with a modified coupled multigrid method whose behaviour within the benchmark problem is also studied numerically.
Copyright © 2001 John Wiley & Sons, Ltd.

KEY WORDS: coupled multigrid methods; higher-order finite element methods; incompressible Navier–Stokes equations

1. INTRODUCTION

The Navier–Stokes equations are a fundamental model in fluid dynamics. There exist a lot of codes that solve these equations numerically. In these codes, many different discretization techniques as well as solvers are implemented. Benchmark problems describing real flow phenomena are important for the evaluation of such codes. A systematic study and comparison of these different discretization and solvers was started within the DFG high priority program 'Flow Simulation with High-Performance Computers' [1]. In this program, benchmark problems for the steady state and the time dependent Navier–Stokes equations were defined. These benchmark problems describe laminar flows around obstacles, i.e. types of flows that can be found in applications. A number of research codes as well as industrial codes solved these benchmark problems. The evaluation of the results brought inside into the

* Correspondence to: Institut für Analysis und Numerik, Otto-von-Guericke-Universität Magdeburg, Postfach 4120, 39016 Magdeburg, Germany.
[1] E-mail: john@mathematik.uni-magdeburg.de

Received 11 February 2000
Revised 28 February 2001

Copyright © 2001 John Wiley & Sons, Ltd.

capabilities of some discretizations and solvers. But a number of questions could not be answered definitely. One of these questions concerns the use of higher-order discretizations [1, p. 565, point 7]: *The use of higher than second order discretizations in space appears promising with respect to the accuracy, but there remains the question of how to solve efficiently the resulting algebraic problems . . . . The results provided for this benchmark are too sparse to allow a definite answer*. In fact, even a second-order discretization was used only in one code. With this code, accurate results were obtained with a relative small number of degrees of freedom.

Higher-order finite element discretizations for the incompressible Navier–Stokes equations are studied analytically, e.g. in [2]. Optimal order error estimates in norms of Sobolev spaces can be proven under certain conditions, especially under the assumption that the solution of the continuous problem is sufficiently smooth. However, this assumption will often not be fulfilled in practice. But on the other hand, norms of Sobolev spaces are in general not of practical interest. Quantities of interest in applications are e.g. mean values of the velocity, and drag or lift coefficients at obstacles. Systematic investigations of the accuracy of different discretizations with respect to such quantities seem to be rare. It is also not known how a missing global regularity of the solution affects the accuracy of higher-order discretizations for local quantities as drag or lift coefficients.

This paper presents a numerical study for several finite element discretizations applied in the benchmark problem 'Flow around a cylinder'. The benchmark parameters are the drag and lift coefficient at the cylinder and the difference of the pressure between the front and the back of the cylinder. The numerical studies show that higher-order isoparametric finite element discretizations show the best accuracy with respect to the benchmark parameters despite the missing smoothness of the solution of the continuous problem.

The discrete problems obtained with higher-order discretizations are solved by a modified coupled multigrid method with Vanka-type smoothers. The modification consists in using stabilized low-order finite element discretizations on the coarser multigrid levels. This solver is described in detail and its behaviour within the benchmark problem is studied for the higher-order finite element discretizations.

2. THE BENCHMARK PROBLEM

This section describes shortly the two-dimensional benchmark problem for the incompressible Navier–Stokes equations defined in [1].

We consider the stationary incompressible Navier–Stokes equations

$$\begin{aligned} -\nu\Delta\mathbf{u} + (\mathbf{u}\cdot\nabla)\mathbf{u} + \nabla p &= \mathbf{0} \quad \text{in } \Omega \\ \nabla\cdot\mathbf{u} &= 0 \quad \text{in } \Omega \\ \mathbf{u} &= \mathbf{g} \quad \text{on } \partial\Omega \end{aligned} \tag{1}$$

with $\nu = 10^{-3}$ m^2 s^{-1} and Ω is the channel shown in Figure 1. The parabolic inflow and outflow profile

Copyright © 2001 John Wiley & Sons, Ltd.

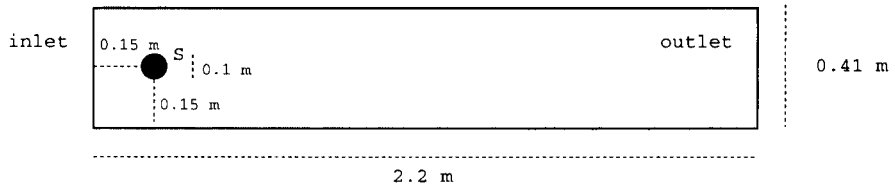

Figure 1. Domain of the benchmark problem.

$$\mathbf{u}(0, y) = \mathbf{u}(2.2, y) = 0.41^{-2}(1.2y(0.41 - y), 0), \quad 0 \le y \le 0.41$$

is prescribed. No-slip conditions are imposed at the other boundaries. Using the mean value of the inflow velocity $U = 0.2$ m s^{-1} and the diameter of the cylinder $L = 0.1$ m as characteristic quantities of the flow, its Reynolds number is $Re = 20$. The density of the fluid is given by $\rho = 1$ kg m^{-3}. An analytical representation of the solution of (1) and its exact regularity are unknown. However, due to the non-convex domain Ω, it is unlikely that $(\mathbf{u}, p)$ is regular enough such that standard error estimates for higher-order finite element discretizations hold, e.g. the pressure has a singularity at the front of the cylinder, see Figure 2.

The benchmark parameters are the drag coefficient c_d at the cylinder, the lift coefficient c_l and the difference of the pressure between the front and the back of the cylinder

$$\Delta p = p(0.15, 0.2) - p(0.25, 0.2)$$

The definition of c_d and c_l is as follows:

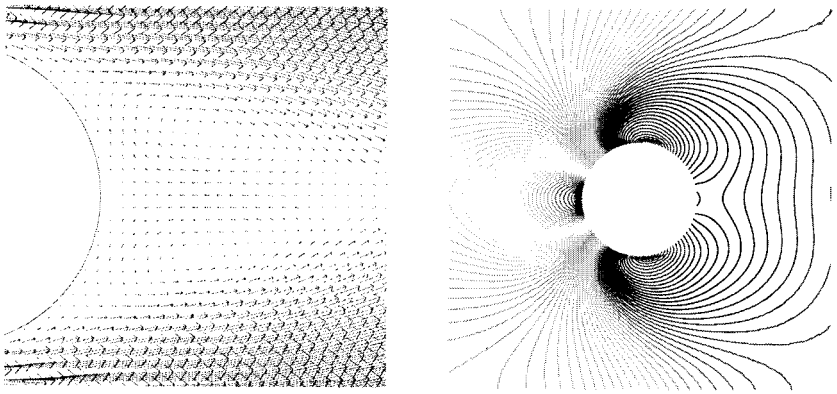

Figure 2. Velocity (left) and pressure (right) at the cylinder.

Copyright © 2001 John Wiley & Sons, Ltd.

$$c_d = \frac{2}{\rho L U^2} \int_S \left(\rho \nu \frac{\partial \mathbf{u}_{t_S}}{\partial n} n_y - p n_x \right) \mathrm{d}S, \qquad c_l = -\frac{2}{\rho L U^2} \int_S \left(\rho \nu \frac{\partial \mathbf{u}_{t_S}}{\partial n} n_x + p n_y \right) \mathrm{d}S \tag{2}$$

Here, $n = (n_x, n_y)^T$ is the normal vector on S directing into Ω, $t_S = (n_y, -n_x)^T$ the tangential vector and $\mathbf{u}_{t_S}$ the tangential velocity.

We have applied in our numerical tests a different computation of these values. This computation starts with choosing an arbitrary function $\mathbf{v}_d \in (H^1(\Omega))^2$ with $(\mathbf{v}_d)|_S = (1, 0)^T$ and $\mathbf{v}_d$ vanishes on all other boundaries. $H^1(\Omega)$ is the usual Sobolev space of order one. The momentum equation in (1) is multiplied with this function and integrated over Ω. One readily verifies that integration by parts and inserting the parameters of the flow yield

$$c_d = -500 \int_\Omega [\nu \nabla \mathbf{u} : \nabla \mathbf{v}_d + (\mathbf{u} \cdot \nabla)\mathbf{u} \cdot \mathbf{v}_d - p(\nabla \cdot \mathbf{v}_d)] \, \mathrm{d}x \tag{3}$$

Similarly, one obtains with $\mathbf{v}_l \in (H^1(\Omega))^2$, $(\mathbf{v}_l)|_S = (0, 1)^T$ and v_l vanishes on the other boundaries

$$c_l = -500 \int_\Omega [\nu \nabla \mathbf{u} : \nabla \mathbf{v}_l + (\mathbf{u} \cdot \nabla)\mathbf{u} \cdot \mathbf{v}_l - p(\nabla \cdot \mathbf{v}_l)] \, \mathrm{d}x \tag{4}$$

In this way, the computation of a line integral on S can be replaced by the computation of volume integrals. Since S is a circular boundary, it is in general approximated in numerical computations by a discrete boundary S_h. Then, the evaluation of (2) is performed on S_h instead of S and it is not clear how much the boundary approximation influences the computed coefficients. We think that in the volume integral formulations (3) and (4) this influence is less than in (2).

Because $\mathbf{v}_d$ and $\mathbf{v}_l$ are up to the boundary conditions arbitrary functions, we can use in the actual computations a finite element function with appropriate boundary conditions. In order to keep the number of integral evaluations in (3) and (4) at a minimum, the functions $\mathbf{v}_d$ and $\mathbf{v}_l$ should have a small support. We used finite element functions of the same order as for the velocity which have the value (1, 0) (or (0, 1)) in all finite element nodes on S_h and vanish in all other modes, see Figure 3 for two examples. Therefore, one has to compute the integrals only in one layer of mesh cells around the cylinder, the shaded mesh cells in Figure 3. From [3] we have the experience that for a non-conforming finite element discretization also a non-conforming finite element function, which does in general not belong to $(H^1(\Omega))^2$, can be used for computing c_d and c_l with (3) and (4), respectively.

3. THE DISCRETE EQUATIONS

3.1. The linearization

The Navier–Stokes equations (1) are linearized by a fixed-point iteration. Given a current iterate $(\mathbf{u}^n, p^n)$, in each iteration step, a linear problem of the form

$$\nu \Delta \mathbf{u}^{n+1} + (\mathbf{u}^n \cdot \nabla)\mathbf{u}^{n+1} + \nabla p^{n+1} = \mathbf{0} \quad \text{in } \Omega$$

Copyright © 2001 John Wiley & Sons, Ltd.

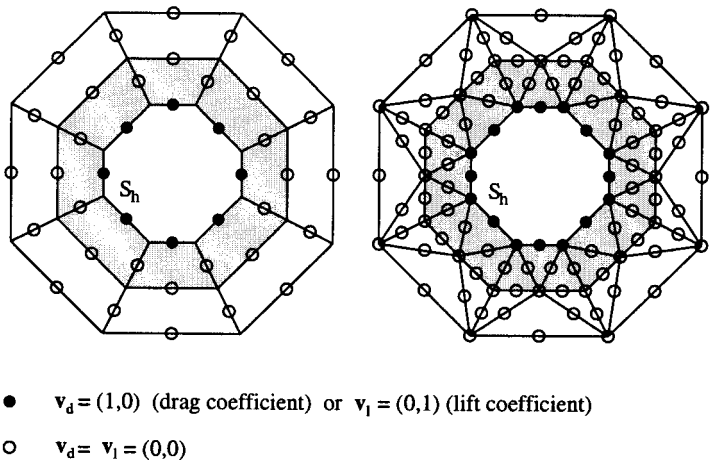

Figure 3. Choice of $\mathbf{v}_d$ and $\mathbf{v}_l$ for Q_1^{rot} velocity (left) and P_2 velocity (right).

$$\nabla \cdot \mathbf{u}^{n+1} = 0 \quad \text{in } \Omega$$

$$\mathbf{u}^{n+1} = \mathbf{g} \quad \text{on } \partial\Omega$$

has to be solved. This boundary value problem is in general convection dominated and is often called the Oseen equation.

3.2. The finite element spaces used in the tests

In this section, we want to introduce the finite element spaces that were used in the tests.

Let $\mathscr{T}_h$ denote a decomposition of Ω into triangles or quadrilaterals and h_K the diameter of the mesh cell K. Let $L^2(\Omega)$ be the Lebesgue space of square integrable functions over the domain Ω with the inner product $(v, w) = \int_\Omega vw \, dx$ and the norm $\|v\|_0 = (v, v)^{1/2}$. The space $H^1(\Omega)$ is equipped with the seminorm $|v|_1 = (\nabla v, \nabla v)^{1/2}$.

We denote by V_h the finite element space for the velocity and by Q_h the finite element space for the pressure. Only such pairs of finite element spaces were involved in the study which fulfil the inf–sup or Babuška–Brezzi stability condition, i.e. there exists a constant $\beta > 0$ independent of the triangulation such that

$$\inf_{q_h \in Q_h} \sup_{\mathbf{v}_h \in V_h} \frac{(\nabla \cdot \mathbf{v}_h, q_h)}{|\mathbf{v}_h|_1 \|q_h\|_0} \geq \beta \tag{6}$$

Condition (6) guarantees the unique solvability of the discrete systems.

First, we consider quadrilateral finite elements. Let $(-1, 1)^2$ be the reference square $\hat{K}$, and F_K the mapping from $\hat{K}$ to an arbitrary quadrilateral K. In general, F_K is a bilinear mapping. Let $Q_k(\hat{K})$ and $P_k(\hat{K})$ be the following sets of polynomials on $\hat{K}$

Copyright © 2001 John Wiley & Sons, Ltd.

$$Q_k(\hat{K}) := \left\{ \hat{q}(\hat{x}_1, \hat{x}_2) = \sum_{i,j=0}^{k} a_{ij} \hat{x}_1^i \hat{x}_2^j \right\}, \qquad P_k(\hat{K}) := \left\{ \hat{p}(\hat{x}_1, \hat{x}_2) = \sum_{0 \le i+j \le k} a_{ij} \hat{x}_1^i \hat{x}_2^j \right\}$$

Then, we define

$$Q_k(K) := \{ q = \hat{q} \circ F_K^{-1} :\ \hat{q} \in Q_k(\hat{K}) \}, \qquad P_k(K) := \{ p = \hat{p} \circ F_K^{-1} :\ \hat{p} \in P_k(\hat{K}) \}$$

and

$$Q_k := \{ v \in H^1(\Omega) :\ v|_K \in Q_k(K) \}, \quad k \ge 1$$

$$Q_0 := \{ v \in L^2(\Omega) :\ v|_K \in Q_0(K) \}$$

$$P_k^{\mathrm{disc}} := \{ v \in L^2(\Omega) :\ v|_K \in P_k(K) \}, \quad k \ge 0$$

In addition, let Q_1^{rot} be the space of non-conforming, mean value oriented, rotated piecewise bilinears defined in [4,5]. We used in our computations the following pairs of quadrilateral finite elements, which fulfil (6):

- $Q_1^{\mathrm{rot}}/Q_0, \quad Q_2/P_1^{\mathrm{disc}}, \quad Q_2/Q_1, \quad Q_3/P_2^{\mathrm{disc}}, \quad Q_3/Q_2$

As usual, the facts that the velocity is a vector valued function and the finite element space of the pressure is intersected with $L_0^2(\Omega)$ are not indicated in these notations. $L_0^2(\Omega)$ denotes the space of functions $q \in L^2(\Omega)$ with $\int_\Omega q \, \mathrm{d}x = 0$.

Now we describe the triangular finite elements we have used. Let us denote for $k \ge 1$ by P_k, the space of continuous piecewise polynomials of degree k, by P_0, the space of piecewise constant functions, and by P_1^{nc}, the space of non-conforming piecewise linears that are continuous at the midpoint of each edge. The reference triangle has the vertices (0, 0), (1, 0) and (0, 1). The following pairs of triangular finite element spaces were involved in our studies:

- $P_1^{\mathrm{nc}}/P_0, \quad P_2/P_1, \quad P_3/P_2$

Since Ω has the non-polygonal boundary part S, the use of isoparametric finite elements seems to be promising. We applied in our studies isoparametric finite element approximations for the Q_2/P_1^{disc}, Q_2/Q_1, P_2/P_1 and P_3/P_2 discretizations.

For more detailed descriptions of the finite element spaces and for references to original papers, see e.g. [6,7].

3.3. The discretizations

We define

$$a(\mathbf{v}, \mathbf{w}) = \sum_{K \in \mathscr{T}_h} \int_K \nabla \mathbf{v} :\ \nabla \mathbf{w} \, \mathrm{d}x, \qquad b(\mathbf{u}, \mathbf{v}, \mathbf{w}) = \sum_{K \in \mathscr{T}_h} \int_K (\mathbf{u} \cdot \nabla) \mathbf{v} \cdot \mathbf{w} \, \mathrm{d}x,$$

$$c(q, \mathbf{v}) = \sum_{K \in \mathscr{T}_h} \int_K q (\nabla \cdot \mathbf{v}) \, \mathrm{d}x$$

Copyright © 2001 John Wiley & Sons, Ltd.

The standard Galerkin discretization of (5) reads as follows:
Given $\mathbf{u}_h^n$, find $(\mathbf{u}_h^{n+1}, p_h^{n+1}) \in V_h \times Q_h$ satisfying $\forall (\mathbf{v}_h, q_h) \in V_h \times Q_h$.

$$va(\mathbf{u}_h^{n+1}, \mathbf{v}_h) + b(\mathbf{u}_h^n, \mathbf{u}_h^{n+1}, \mathbf{v}_h) - c(p_h^{n+1}, \mathbf{v}_h) = \mathbf{0}$$

$$c(q_h, \mathbf{u}_h^{n+1}) = 0 \tag{7}$$

Since (5) is, in general, a convection-dominated equation, the application of stabilization techniques with respect to the convective term may be useful for some discretizations.

As one stabilization technique, we applied the streamline diffusion finite element method (SDFEM) which was introduced in [8,9] and analyzed for Navier–Stokes equations, e.g. in [10,11]. The weak formulation reads as follows:
Given $\mathbf{u}_h^n$, find $(\mathbf{u}_h^{n+1}, p_h^{n+1}) \in V_h \times Q_h$ satisfying $\forall (\mathbf{v}_h, q_h) \in V_h \times Q_h$

$$va(\mathbf{u}_h^{n+1}, \mathbf{v}_h) + b(\mathbf{u}_h^n, \mathbf{u}_h^{n+1}, \mathbf{v}_h) - c(p_h^{n+1}, \mathbf{v}_h)$$
$$+ \sum_{K \in \mathscr{T}_h} \delta_K \int_K (v \Delta \mathbf{u}_h^{n+1} + (\mathbf{u}_h^n \cdot \nabla)\mathbf{u}_h^{n+1} + \nabla p_h^{n+1})((\mathbf{u}_h^n \cdot \nabla)\mathbf{v}_h)\, \mathrm{d}x = \mathbf{0}$$

$$c(q_h, \mathbf{u}_h^{n+1}) = 0 \tag{8}$$

We used the streamline diffusion parameter $\delta_K = h_K^2$.

A second stabilization scheme which is involved in our study is an upwind discretization which was investigated in [5,12] for non-conforming finite element spaces of lowest order. This type of stabilization is used only in connection with the finite element spaces Q_1^{rot}/Q_0 and P_1^{nc}/P_0. The upwind finite element discretization of (5) reads as follows:
Given $\mathbf{u}_h^n$, find $(\mathbf{u}_h^{n+1}, p_h^{n+1}) \in V_h \times Q_h$ satisfying $\forall (\mathbf{v}_h, q_h) \in V_h \times Q_h$

$$va(\mathbf{u}_h^{n+1}, \mathbf{v}_h) + \tilde{b}(\mathbf{u}_h^n, \mathbf{u}_h^{n+1}, \mathbf{v}_h) - c(p_h^{n+1}, \mathbf{v}_h) = \mathbf{0}$$

$$c(q_h, \mathbf{u}_h^{n+1}) = 0 \tag{9}$$

where, see Figure 4

$$\tilde{b}(\mathbf{u}, \mathbf{v}, \mathbf{w}) = \sum_{i=1}^{N} \sum_{j \in \Lambda_i} \int_{\Gamma_{ij}} (\mathbf{u} \cdot \mathbf{n}_{ij})(1 - \lambda_{ij}(\mathbf{u}))(\mathbf{v}(B_j) - \mathbf{v}(B_i)) \cdot \mathbf{w}(B_i)\, \mathrm{d}s$$

Here, N is the number of degrees of freedom of the velocity, Λ_i is the set of all indices for which the nodes B_i and B_j belong to the same mesh cell, Γ_{ij} is the edge to node B_j of the dual

Copyright © 2001 John Wiley & Sons, Ltd.

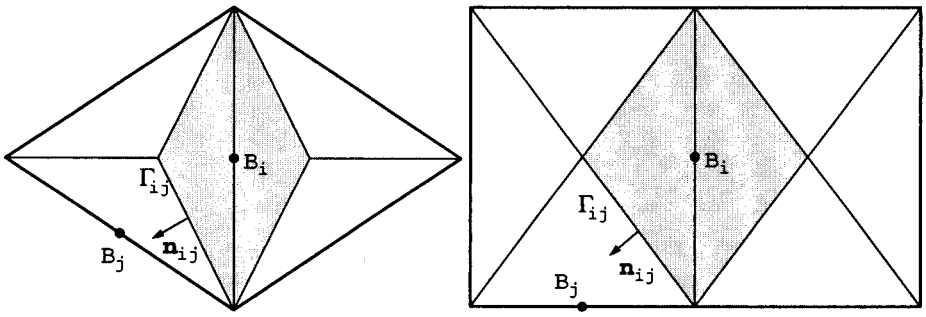

Figure 4. Dual domains for computing the upwind discretization, P_1^{nc} velocity (left), Q_1^{rot} velocity (right).

mesh cell around node B_i (shaded in Figure 4) and $\mathbf{n}_{ij}$ is the outward directing normal at Γ_{ij}. Let

$$t = \frac{1}{2\nu} \int_{\Gamma_{ij}} \mathbf{u} \cdot \mathbf{n}_{ij} \, \mathrm{d}s$$

then the weighting function is defined by

$$\lambda_{ij}(\mathbf{u}) = \Phi(t) = \begin{cases} \dfrac{1+2t}{2+2t} & \text{if } t \geq 0 \\ \dfrac{1}{2-2t} & \text{if } t < 0 \end{cases}$$

The upwind method with this weighting function is called Samarskij upwind. A simpler upwind discretization, the so-called sharp upwind discretization produced very inaccurate results. This was already observed in [1, p. 565, point 5].

All integrals are evaluated by a transformation to the reference element and the application of a quadrature rule on the reference element. This quadrature rule is exact for all polynomials that occur in the bi- and trilinear forms for a given pair of finite element spaces. Thus, integrals on mesh cells that have an affine transformation to the reference element are computed exactly. If the transformation from the reference element to a mesh cell is bilinear or isoparametric, there is a quadrature error due to the non-polynomial inverse reference transformation.

4. THE MULTIGRID SOLVER

We applied a (strongly) coupled multigrid method for the solution of the discrete Oseen problems. The evaluation of the benchmark computations [1, p. 564, point 2], showed that

Copyright © 2001 John Wiley & Sons, Ltd.

coupled multigrid methods are among the best classes of solvers known so far for this type of equations. The algebraic form of the discrete Oseen equations looks as follows:

$$\mathscr{A}\begin{pmatrix} u \\ p \end{pmatrix} = \begin{pmatrix} A & B \\ C & 0 \end{pmatrix}\begin{pmatrix} u \\ p \end{pmatrix} = \begin{pmatrix} f \\ g \end{pmatrix} \tag{10}$$

We applied the coupled multigrid method with local smoothers, so-called Vanka-type smoothers [13]. The behaviour of these methods has been studied numerically for non-conforming finite element spaces of first-order in a number of papers [14–17]. In these studies, they behaved superior to several other classes of solvers.

Vanka-type smoothers can be considered as block Gauss–Seidel methods. Let $\mathscr{V}_h$ and $\mathscr{Q}_h$ be the set of velocity and pressure degrees of freedom (d.o.f.) respectively. These sets are decomposed into

$$\mathscr{V}_h = \bigcup_{j=1}^{J} \mathscr{V}_{hj}, \qquad \mathscr{Q}_h = \bigcup_{j=1}^{J} \mathscr{Q}_{hj} \tag{11}$$

The subsets are not required to be disjoint.

Let $\mathscr{A}_j$ be the block of the matrix $\mathscr{A}$ which is connected with the degrees of freedom of $\mathscr{W}_{hj} = \mathscr{V}_{hj} \cup \mathscr{Q}_{hj}$, i.e. the intersection of the rows and columns of $\mathscr{A}$ with the global indices belonging to $\mathscr{W}_{hj}$

$$\mathscr{A}_j = \begin{pmatrix} A_j & B_j \\ C_j & 0 \end{pmatrix} \in \mathbb{R}^{\dim(\mathscr{W}_{hj}) \times \dim(\mathscr{W}_{hj})}$$

In addition, we define

$$\mathscr{D}_j = \begin{pmatrix} \operatorname{diag}(A_j) & B_j \\ C_j & 0 \end{pmatrix} \in \mathbb{R}^{\dim(\mathscr{W}_{hj}) \times \dim(\mathscr{W}_{hj})}$$

Similarly, we denote by $(\cdot)_j$ the restriction of a vector on the rows corresponding to the degrees of freedom in $\mathscr{W}_{hj}$. The *diagonal Vanka smoother* updates the velocity and pressure values connected to $\mathscr{W}_{hj}$ by

$$\begin{pmatrix} u \\ p \end{pmatrix}_j := \begin{pmatrix} u \\ p \end{pmatrix}_j + \mathscr{D}_j^{-1}\left(\begin{pmatrix} f \\ g \end{pmatrix} - \mathscr{A}\begin{pmatrix} u \\ p \end{pmatrix}\right)_j$$

The *full Vanka smoother* computes new velocity and pressure values by

$$\begin{pmatrix} u \\ p \end{pmatrix}_j := \begin{pmatrix} u \\ p \end{pmatrix}_j + \mathscr{A}_j^{-1}\left(\begin{pmatrix} f \\ g \end{pmatrix} - \mathscr{A}\begin{pmatrix} u \\ p \end{pmatrix}\right)_j$$

Copyright © 2001 John Wiley & Sons, Ltd.

We have applied two types of Vanka smoothers with respect to the decomposition (11). The first type is called *mesh cell oriented*. For this type of smoother, J is the number of mesh cells and $\mathcal{W}_{hj}$ are the degrees of freedom which are connected to the mesh cell j. This approach works only for finite element spaces with discontinuous discrete pressure. In the *pressure node oriented Vanka smoother*, J is the global number of pressure degrees of freedom, $\dim \mathcal{Q}_{hj} = 1$ for all j, and V_{hj} is the set of velocity degrees of freedom which are connected to the pressure degree of freedom of $\mathcal{Q}_{hj}$ in the matrix C. Obviously, for a piecewise constant discrete pressure, the mesh cell oriented and the pressure node oriented Vanka smoother are equivalent. The linear systems with the diagonal pressure node oriented Vanka smoother can be solved very fast by applying two inner vector products whereas for the systems with the other Vanka smoothers the Gaussian algorithm with pivoting is used in our tests.

The prolongation in the multigrid method is based on so-called nodal functionals. On each mesh cell K there exists a local finite element basis $\{\varphi_i^K\}$ and a dual basis $\{N_i^K\}$ of nodal functionals such that

$$N_i^K(\varphi_j^K) = \delta_{ij}$$

where δ_{ij} is the Kronecker delta. Let $\{\varphi_j : j \in J\}$ be the basis of the finite element space. The indices j are called nodes or global degrees of freedom. Let I_j be the set of all pairs (K, i) of local degrees of freedom, which forms a global degree of freedom, see Figure 5. Then, the global nodal functional of a piecewise given function v is defined as a weighted average of the local nodal functionals

$$N_j(v) := \frac{1}{|I_j|} \sum_{(K,i) \in I_j} N_i^K(v)$$

Let V_l be the finite element space on multigrid level l and V_{l+1} the finite element space on the next finer level $l+1$. The prolongation of $v_l \in V_l$ into V_{l+1} is given via

$$v_{l+1} = \sum_{i=1}^{\dim(V_{l+1})} N_i(v_l)\varphi_i$$

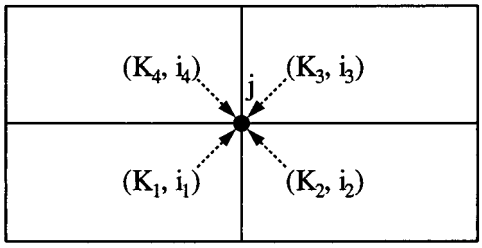

Figure 5. Node j with cell wise contributions (K_m, i_m), $I_j = \cup_{m=1}^{4}(K_m, i_m)$.

Copyright © 2001 John Wiley & Sons, Ltd.

where $\{\varphi_i\}$ is the basis of V_{l+1}. Note, it is not necessary that the spaces V_l and V_{l+1} are based on the same finite element. This fact is exploited in the modified multigrid method described below. Analytical properties of this prolongation operator are studied in [18].

It was impossible for some discretizations to solve the linear system (10) with the (standard) approach of using on all multigrid levels the same discretization. The multigrid solver showed the best efficiency for the first-order non-conforming finite element discretizations with Samarskij upwind. For this reason, we used a modified multigrid approach, see Figure 6. Let L be the finest level of the geometric grid hierarchy. Then, the finest level of the multigrid hierarchy is $L+1$. The multigrid levels L and $L+1$ are connected both to the geometric level L. The discretization in the study is applied on the multigrid level $L+1$, whereas on all other levels a lowest-order non-conforming discretization with Samarskij upwind stabilization is used. Sensible parameters in this approach are the damping factor for the smoother on multigrid level $L+1$ and the damping factor of the prolongation from level L to $L+1$.

5. NUMERICAL STUDIES

In this section, we present the numerical results with respect to the accuracy of the computed benchmark parameters and the behaviour of the coupled multigrid solver for the different discretizations.

The initial grids presented in Figure 7 are used in the numerical tests. The quadrilateral grid consists of 208 mesh cells and the triangular grid of 388. Both initial grids posses fine mesh cells around the cylinder. Such *a priori* adapted grids have been proven to lead to accurate

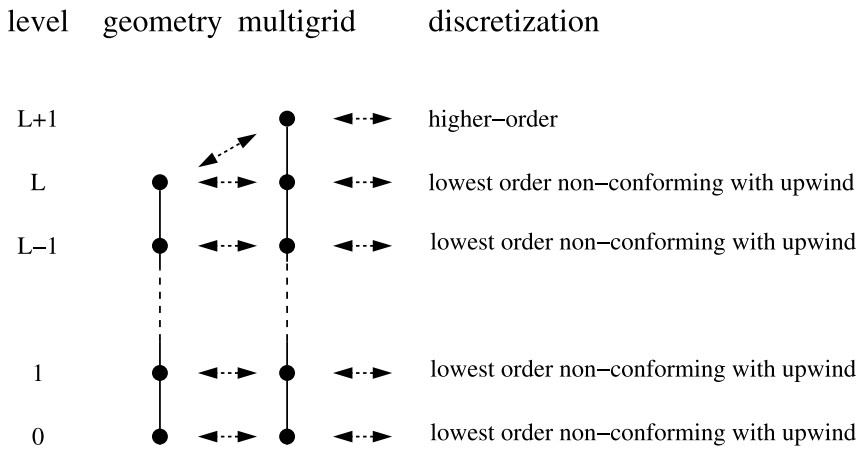

Figure 6. The modified multigrid approach for higher-order discretizations.

Copyright © 2001 John Wiley & Sons, Ltd.

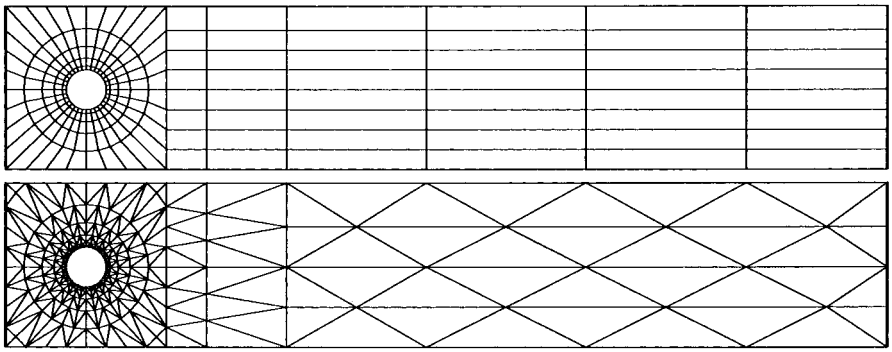

Figure 7. Coarsest grids for the benchmark problem.

solutions, see [1, p. 565, point 9]. Also, *a posteriori* adaptively refined grids that are based on error estimators for the benchmark parameters are highly refined at the cylinder, see [19,20].

All computations were carried out with the code MooNMD2.2 [21].

5.1. The accuracy of the discretizations

The computed drag coefficients and pressure differences are compared with reference values obtained with a high-order spectral method [22, p. 74]

$$c_{\mathrm{d,ref}} = 5.57953523384, \qquad \Delta p_{\mathrm{ref}} = 0.11752016697$$

These reference values coincide quite well with extrapolations of computed values in our study. For the lift coefficient, however, we used

$$c_{\mathrm{l,ref}} = 0.010618937712$$

as reference value which differs a little bit from the value 0.010618948146 given in [22]. We have obtained $c_{\mathrm{l,ref}}$ by extrapolating the results of the isoparametric P_3/P_2 finite element discretization.

The errors of the computed values to these reference values are presented graphically in Figures 8–10. These plots contain also the asymptotics for second- and fourth-order convergence. The different pairs of finite element spaces are plotted by different line styles. The different discretizations are distinguished by different markers:

+, Galerkin discretization, isoparametric finite elements;
○, Galerkin discretization, polygonal boundary approximation;
*, SDFEM discretization, polygonal boundary approximation;
△, Samarskij upwind discretization, polygonal boundary approximation.

Copyright © 2001 John Wiley & Sons, Ltd.

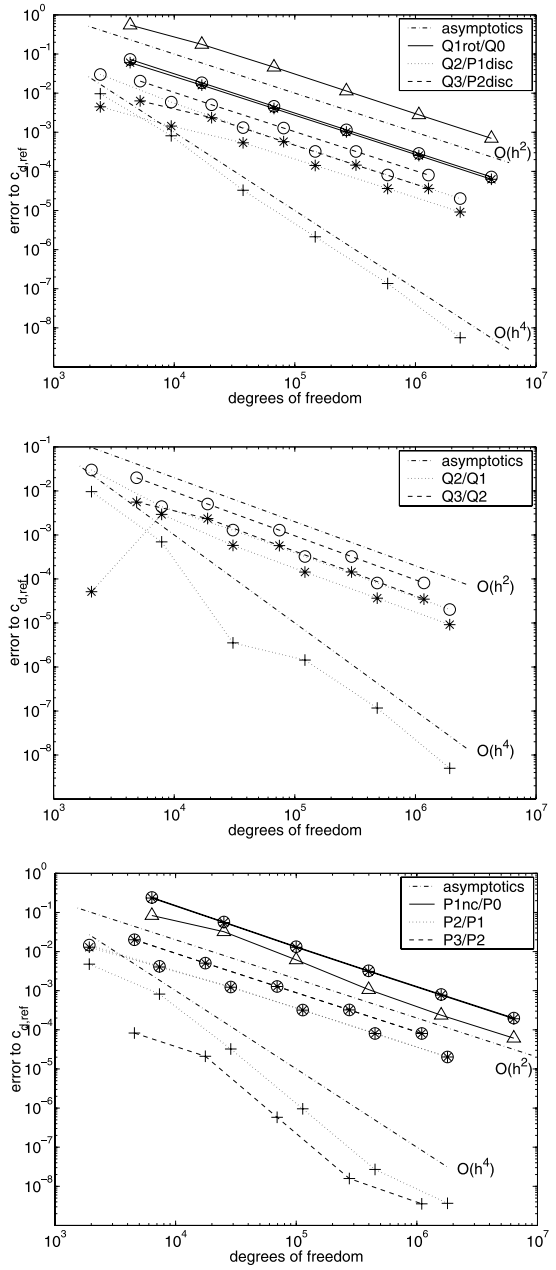

Figure 8. Errors of the computed drag coefficients to $c_{\mathrm{d,ref}}$ ($+$, isoparametric Galerkin; $\bigcirc$, polygonal Galerkin; *, polygonal SDFEM; $\triangle$, polygonal Samarskij).

Copyright © 2001 John Wiley & Sons, Ltd.

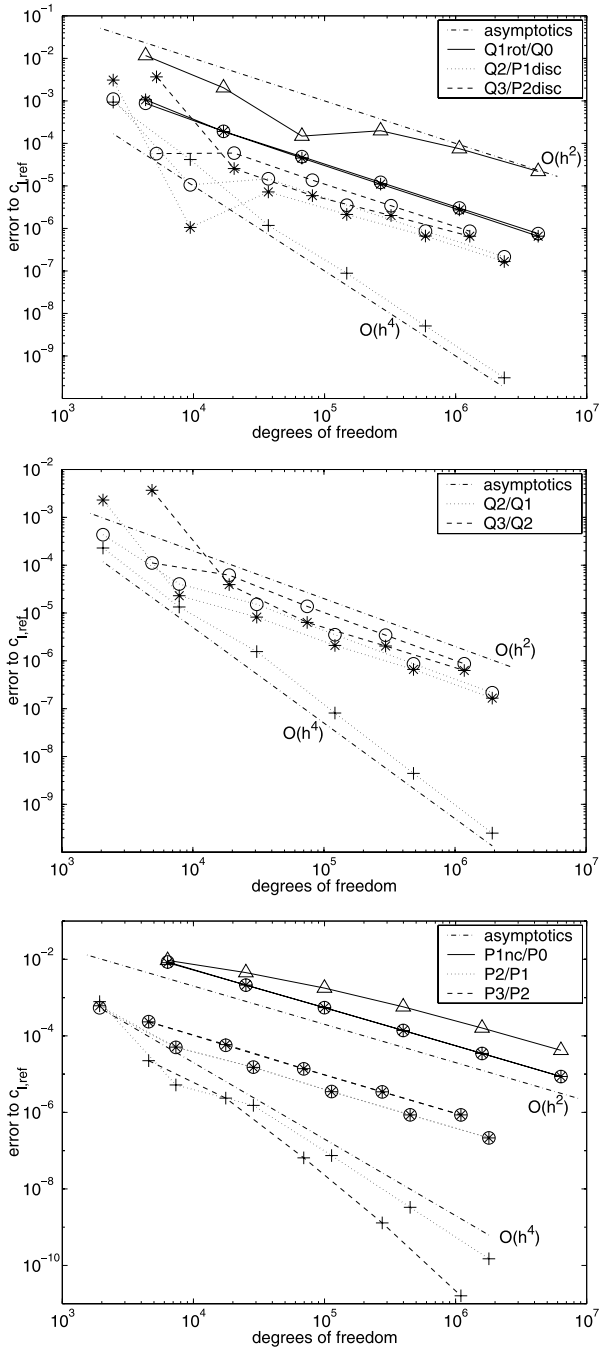

Figure 9. Errors of the computed lift coefficients to $c_{\mathrm{l,ref}}$ ($+$, isoparametric Galerkin; $\bigcirc$, polygonal Galerkin; *, polygonal SDFEM; $\triangle$, polygonal Samarskij).

Copyright © 2001 John Wiley & Sons, Ltd.

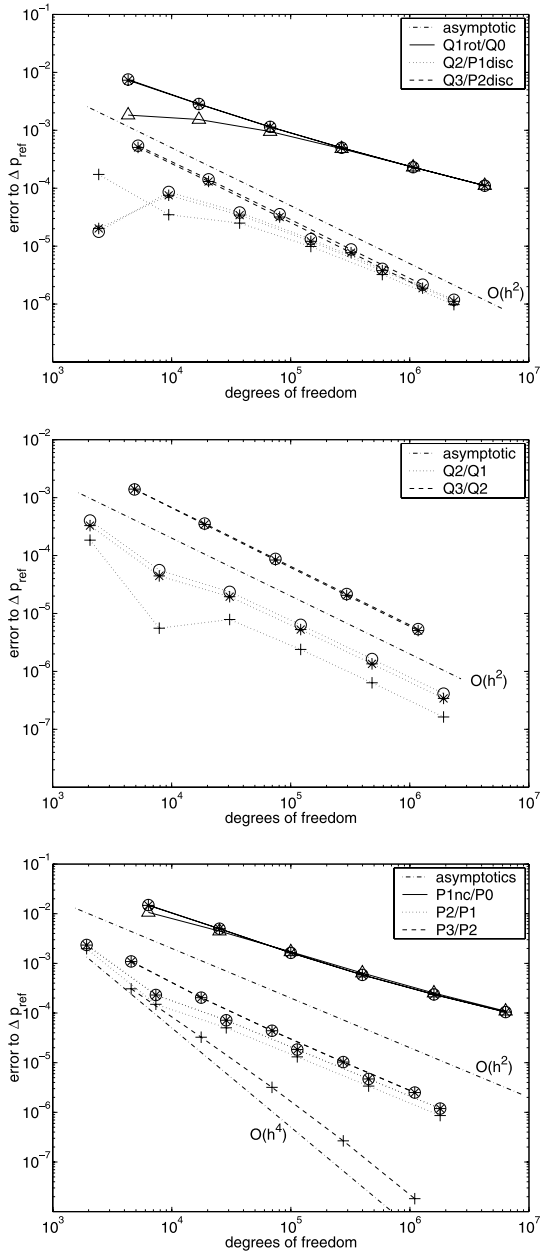

Figure 10. Errors of the computed pressure difference to Δp_{ref} (+ , isoparametric Galerkin; ○, polygonal Galerkin; *, polygonal SDFEM; △, polygonal Samarskij).

Copyright © 2001 John Wiley & Sons, Ltd.

For discontinuous discrete pressure, Δp was computed by averaged values at the front and the back of the cylinder, respectively. If possible, the discrete non-linear systems were solved on each level up to an Euclidean norm of the residual of 10^{-15}. However, this stopping criterion could often not be reached for the discretizations on quadrilateral grids. The quadrature errors mentioned in Section 3.3 may cause that the conservation of mass in the discrete equations is violated somewhat. In these computations, we relaxed the stopping criterion to 10^{-12}, which was always reached.

By far the most accurate results are obtained with second- and third-order isoparametric finite element discretizations. The better quality of the boundary approximation improves the accuracy of the computed benchmark values very much in comparison to the polygonal approximation of S. Second- and third-order discretizations with polygonal discrete boundary give similar results. The main error comes from the crude boundary approximation. The use of the streamline–diffusion stabilization influences the results only marginally. The used grids seem to be already in the asymptotic regime such that the effect of the streamline-diffusion stabilization is negligible. By far the most inaccurate results are obtained with the lowest-order non-conforming discretizations.

The numerical results provide some additional observations which are also noteworthy. For instance, only the isoparametric P_3/P_2 finite element discretization shows a higher than second-order convergence for Δp, see Figure 10. Also, the accuracy of the computed values on quadrilateral and triangular grids for a similar number of degrees of freedom is not much different. Thus, from our tests there is no reason to prefer one of these grid types from the point of view of accuracy.

The numerical results suggest that each benchmark parameter has a well-defined order of convergence which depends on the discretization. However, to our knowledge there are no rigorous analytical convergence proofs available in the literature.

5.2. The behaviour of the modified coupled multigrid method

Table I illustrates the behaviour of the modified coupled multigrid method for the higher-order discretizations. The initial guess for the non-linear iteration was the interpolated solution from the previous level and the iteration was stopped for an Euclidean norm of the residual less than 10^{-10}. For the solution of the linear saddle point problems (10), at most 10 multigrid cycles were applied or this iteration was stopped after a reduction of the norm of the residual by the factor 10. The systems on the coarsest grid were solved approximately by 100 iterations with the smoother. We found that a moderate damping of the smoother on the multigrid level $L+1$ as well as for the prolongation from level L to $L+1$ was sufficient for the multigrid method applied to discretizations with discontinuous pressure. Both damping factors were set to 0.8 in the computations presented in Table I. In the computations with continuous pressure, both damping factors are set to 0.4. This stronger damping was often necessary in order to achieve the convergence of the solver. Since the behaviour for a certain pair of finite element spaces was quite similar with respect to all discretizations, only the results for the most accurate discretization are given. The $W(2, 2)$-, $W(3, 3)$- and $W(4, 4)$-cycles were tested for the combinations of pairs of finite element spaces and Vanka-type smoothers and the best result (fastest

Copyright © 2001 John Wiley & Sons, Ltd.

Table I. The behaviour of the modified coupled multigrid method (fixed point iterations/multigrid cycles and computing time).

FE space (discretization)	$L+1$	d.o.f.	Cycle	Smoother	Iterations	Time
Q_2/P_1^{disc} (isoparametric)	5	588 160	$W(3,3)$	Cell, full	5/11	554
			$W(4,4)$	Cell, diag	5/22	1141
			$W(3,3)$	Node, full	5/11	952
Q_2/Q_1 (isoparametric)	5	482 272	$W(2,2)$	Node, full	6/44	5612
P_2/P_1 (isoparametric)	5	449 856	$W(2,2)$	Node, full	7/55	4338
			$W(4,4)$	Node, diag	8/64	3251
Q_3/P_2^{disc} (Galerkin)	4	321 312	$W(2,2)$	Cell, full	10/39	891
			$W(2,2)$	Cell, diag	10/50	1038
			$W(2,2)$	Node, full	9/35	2819
Q_3/Q_2 (Galerkin)	4	295 296	$W(2,2)$	Node, full	8/67	16 578
P_3/P_2 (isoparametric)	4	275 456	$W(3,3)$	Node, full	5/29	4359
			$W(3,3)$	Node, diag	8/65	3043

computation time) is reported in Table I. The computations were carried out on a HP workstation with PA-8500 processor (440 MHz, 1760 Mflop s^{-1} peak performance).

In Table I, we give the number of fixed-point iterations, the total number of multigrid cycles, and the computing times in seconds for the solution of the discrete Navier–Stokes equations. The results show that the modified multigrid method works most efficient for finite element spaces with discontinuous pressure. The best behaviour can be observed for the combination of the Q_2/P_1^{disc} finite element space and the full mesh cell oriented Vanka smoother. The multigrid method with the diagonal pressure node oriented Vanka smoother did not converge for these pairs of finite element spaces.

As mentioned in Section 4, only pressure node oriented Vanka smoothers are used for finite element spaces with continuous pressure. It can be seen from Table I that the modified multigrid method behaved differently for discretizations on triangular and quadrilateral meshes. It had no problems to converge for the P_2/P_1 and P_3/P_2 pairs of finite element spaces. The diagonal pressure node oriented Vanka smoother was more efficient than its full counterpart. The most difficulties in the solution of the discrete problems were encountered for the higher-order finite element spaces with continuous pressure on quadrilateral grids. The modified multigrid method with the diagonal pressure node oriented Vanka smoother did not converge in these cases. The loss of information in replacing $\mathscr{A}_j$ by $\mathscr{D}_j$ is apparently too large here. Also the computation times with the full pressure node oriented Vanka smoother are large in comparison to the other pairs of finite element spaces.

The results given in Table I provide some insight into the behaviour of the modified coupled multigrid method. The study of this method applied in the solution of high Reynolds number flows, flows in more complex domains and time dependent flows will be the subject of a forthcoming study.

Copyright © 2001 John Wiley & Sons, Ltd.

5.3. Conclusions

We want to summarize the most important conclusions of the numerical tests within the benchmark problem 'Flow around a cylinder':

- By far the most accurate benchmark parameters are obtained with isoparametric higher-order discretizations although the solution of the continuous problem is not of higher regularity.
- There could be obtained more accurate results with all higher-order discretizations in less computing time and with less memory than with the low-order non-conforming discretizations.
- The importance of the low-order discretizations lies in the possibility of constructing modified multigrid solvers for higher-order discretizations as described in Section 4.
- The modified coupled multigrid method worked best for higher-order finite element spaces with discontinuous discrete pressure.
- The isoparametric Q_2/P_1^{disc} discretization proved to be best concerning both the accuracy of the discrete solution and the efficient solvability of the discrete systems. Among the discretizations on triangular grids, the isoparametric P_2/P_1 and the isoparametric P_3/P_2 discretization worked equally well.

ACKNOWLEDGMENTS

The work of the second author was supported by the Deutsche Forschungsgemeinschaft (DFG) by grant En278/2-1. Figure 2 was plotted using the software package GRAPE.

REFERENCES

1. Schäfer M, Turek S. The benchmark problem 'Flow around a cylinder'. In *Flow Simulation with High-Performance Computers II. Notes on Numerical Fluid Mechanics*, vol. 52, Hirschel EH (ed.). Vieweg: Wiesbaden, 1996; 547–566.
2. Girault V, Raviart P-A. *Finite Element Methods for Navier–Stokes Equations*. Springer: Berlin, 1986.
3. John V. Parallele Lösung der inkompressiblen Navier–Stokes Gleichungen auf adaptiv verfeinerten Gittern. PhD thesis, Otto-von-Guericke-Universität Magdeburg, Fakultät für Mathematik, 1997.
4. Rannacher R, Turek S. Simple nonconforming quadrilateral Stokes element. *Numerical Methods for Partial Differential Equations* 1992; **8**: 97–111.
5. Schieweck F. Parallele Lösung der stationären inkompressiblen Navier–Stokes Gleichungen. Otto-von-Guericke-Universität Magdeburg, Fakultät für Mathematik, Habilitation, 1997.
6. Brezzi F, Fortin M. Mixed and hybrid finite element methods. In *Springer Series in Computational Mathematics*, vol. 15. Springer: Berlin, 1991.
7. Fortin M. Finite element solution of the Navier–Stokes equations. *Acta Numerica* 1993: 239–284.
8. Hughes TJR, Brooks AN. A multidimensional upwind scheme with no crosswind diffusion. In *Finite Element Methods for Convection Dominated Flows*, *AMD*, vol. 34, Hughes TJR (ed.). ASME: New York, 1979; 19–35.
9. Brooks AN, Hughes TJR. Streamline upwind/Petrov–Galerkin formulations for convection dominated flows with particular emphasis on the incompressible Navier–Stokes equations. *Computer Methods in Applied Mechanics and Engineering* 1982; **32**: 199–259.
10. Lube G, Tobiska L. A nonconforming finite element method of streamline-diffusion type for the incompressible Navier–Stokes equation. *Journal of Computational Mathematics* 1990; **8**: 147–158.
11. Tobiska L, Verfürth R. Analysis of a streamline diffusion finite element method for the Stokes and Navier–Stokes equations. *SIAM Journal of Numerical Analysis* 1996; **33**(1): 107–127.
12. Schieweck F, Tobiska L. An optimal order error estimate for an upwind discretization of the Navier–Stokes equations. *Numerical Methods for Partial Differential Equations* 1996; **12**: 407–421.

Copyright © 2001 John Wiley & Sons, Ltd.

13. Vanka S. Block-implicit multigrid calculation of two-dimensional recirculating flows. *Computer Methods in Applied Mechanics and Engineering* 1986; **59**(1): 29–48.
14. Turek S. Efficient solvers for incompressible flow problems: an algorithmic and computational approach. In *Lecture Notes in Computational Science and Engineering*, vol. 6. Springer: Berlin, 1999.
15. John V. A comparison of parallel solvers for the incompressible Navier–Stokes equations. *Computing and Visualization in Science* 1999; **4**(1): 193–200.
16. John V, Tobiska L. Smoothers in coupled multigrid methods for the parallel solution of the incompressible Navier–Stokes equations. *International Journal for Numerical Methods in Fluids* 2000; **33**: 453–473.
17. John V, Matthies G, Mitkova TI, Tobiska L, Vassilevski PS. A comparison of three solvers for the incompressible Navier–Stokes equations. In *Large-Scale Scientific Computations of Engineering and Environmental Problems. Notes on Numerical Fluid Mechanics*, vol. 73, Griebel M, Margenov SD, Yalamov P (eds). Vieweg: Wiesbaden, 2000; 215–222.
18. Schieweck F. A general transfer operator for arbitrary finite element spaces. Preprint 25, Fakultät für Mathematik, Otto-von-Guericke-Universität Magdeburg, 2000.
19. Becker R. Weighted error estimators for finite element approximations of the incompressible Navier–Stokes equations. Universität Heidelberg. Preprint 48/98, 1998.
20. Becker R, Rannacher R. Weighted a posteriori error control in fe methods. In *ENUMATH 97, Proceedings of the 2nd European Conference on Numerical Mathematics and Advanced Applications*, Bock HG, *et al*. (eds). World Scientific Publishing Company: Singapore, 1996; 621–637.
21. Behns V, John V, Matthies G, Schieweck F. *MooNMD2.2.* Otto-von-Guericke-Universität Magdeburg, Institut für Analysis und Numerik, 2001.
22. Nabh G. On higher order methods for the stationary incompressible Navier–Stokes equations. PhD thesis, Universität Heidelberg. Preprint 42/98, 1998.

Copyright © 2001 John Wiley & Sons, Ltd.